J. Space Weather Space Clim. 2022, **12**, 13
© C. Jiang et al., Published by EDP Sciences 2022
https://doi.org/10.1051/swsc/2022010

JSWSC

Available online at:
www.swsc-journal.org

Topical Issue - Ionospheric plasma irregularities and their impact on radio systems

RESEARCH ARTICLE OPEN ACCESS

Upwelling coherent backscatter plumes observed with ionosondes in low-latitude region

Chunhua Jiang[1,*], Lehui Wei[1], Tatsuhiro Yokoyama[2], Jiyao Xu[3,4], Kun Wu[3,4], Wei Yuan[3,4], Jing Liu[5], Tongxin Liu[1], Guobin Yang[1], and Zhengyu Zhao[1]

[1] School of Electronic Information, Wuhan University, Wuhan, Hubei 430072, China
[2] Research Institute for Sustainable Humanosphere, Kyoto University, Uji 606-8501, Japan
[3] State Key Laboratory of Space Weather, National Space Science Center, Chinese Academy of Sciences, Beijing 100190, China
[4] College of Earth Sciences, University of the Chinese Academy of Sciences, Beijing 100049, China
[5] Institute of Earthquake Science, China Earthquake Administration, Beijing 100036, China

Received 21 September 2021 / Accepted 31 March 2022

Abstract – Investigations of upwelling backscatter plumes are mostly from observations of VHF radars. This study reports the first observation of upwelling backscatter plumes (backscatter echoes beyond the critical frequency of the F2 layer, foF2) recorded by ionosondes at low latitudes on 13 March 2015. With a pair of ionosondes (Puer, 22.7° N, 101.05° E, Dip Lat 12.9° N, and Chiang Mai, 18.76° N, 98.93° E, Dip Lat 9.04° N), Swarm satellites flying side-by-side (longitudinal separation of about 1.4°, about 150 km), and an all-sky imager (25° N, 104° E, Dip Lat 15.1° N), the evolution of plasma bubbles is presented in this study. Observations show that ionosonde backscatter plumes originating from a local-scale upwelling could be observed. In addition, this study also reported ionosonde backscatter plumes from other regions with approaching and receding characteristics. Results show that characteristics of backscatter plumes with ionosondes are consistent with observations from VHF radars. It suggests that ionosonde backscatter plumes might also be used to study the characteristics of upwelling backscatter plumes.

Keywords: Upwelling backscatter plumes / plasma bubbles / ionosonde backscatter plumes / spread F

1 Introduction

The structure and characteristics of spread F/plasma bubbles are mostly from VHF and UHF radar observations of backscatter plumes (Woodman & La Hoz, 1976; Kelley et al., 1981; Tsunoda, 1981, 1983; Fukao et al., 2003; Otsuka et al., 2004; Yokoyama & Fukao, 2006; Li et al., 2016). Kelley et al. (1981) reported backscatter plumes associated with spread F by the Jicamarca radar and the two oscillations (two full cycles of modulated apparent vertical drift) in the altitude-time intensity. They found that the asymmetry of plumes formation might be induced by the zonal neutral wind. With a beam-scanning technology in the radar system, multi-beam observations of backscatter plumes could provide a good opportunity to study the spatial structure of plasma bubbles/depletions. Later, Tsunoda (1981, 1983) studied the time evolution and structure of the backscatter plumes by ALTAIR (the VHF radar operated at 155.5 MHz) located in the Marshall Islands. Tsunoda found that backscatter strength increases (the phase of upward development) and decreases (upward plume growth slows or ceases) in the different phases of the plumes. Tsunoda (1983) further pointed out that an east–west asymmetry structure in plasma bubbles can be explained by eastward neutral winds. Furthermore, the unstable west wall of the depletions/bubbles (upwelling) could produce secondary plumes. Yokoyama & Fukao (2006) reported the first observation of upwelling backscatter plumes in the growth phase of equatorial spread F with the equatorial atmosphere radar (EAR) and estimated the velocity of the upwelling plumes (a few tens to a few hundreds of meters per second). Moreover, Tsunoda (2015) suggested that the upwelling might be a unit of disturbance (whose presence is responsible for the formation of equatorial spread F) and claimed that small-scale irregularities (less than 1 km) might be excited along the west wall of the upwelling. Therefore, investigation of the upwelling backscatter plumes associated with the spread F/plasma bubble might play a significant role in identifying the sources of the spread F/plasma bubble.

It is well known that there is one type of spread F (strong range spread F) on ionograms where echoes can extend beyond the critical frequency of the F2 layer (foF2) (Argo & Kelley, 1986; Sales et al., 1996; Wright et al., 1996; Shi et al., 2011;

*Corresponding author: chuajiang@whu.edu.cn

Abdu et al., 2012). Argo & Kelley (1986) reported equatorial spread F and suggested the ionosonde may, in fact, function as a coherent scatter radar at frequencies above the nominal foF2. Sales et al. (1996) studied spread F and the structure of plasma bubbles in the southern anomaly region by optical and radio sensors. They found that the field-aligned F region irregularities within plasma bubbles (the walls of the depletion) could produce strong coherent backscatter echoes on the ionograms, especially for the echoes beyond foF2. Additionally, Wright et al. (1996) found that the total-reflection interpretation of ionogram spread F is consistent with rocket and satellite data, especially for the intense, broadband, and flat features of equatorial ionograms spread F. Recently, Abdu et al. (2012) further pointed out that the ESF trace from ionosonde is found to be consistent with the echoes from coherent backscattering. It is well known that the echoes on ionograms are complicated. In this case study, we think that if the echoes are total-reflection, the corresponding electron density should be larger than the background (plasma blob). Otherwise, we think that the echoes beyond the foF2 are mainly from coherent backscattering. This case study did not find the larger density (plasma blobs) but plasma depletions (bubbles) by satellites observations compared with the background density. Therefore, we think the echoes beyond the foF2 in this case study are from coherent backscattering.

In this study, backscatter echoes beyond the foF2 on ionograms (Argo & Kelley, 1986; Sales et al., 1996; Wright et al., 1996; Shi et al., 2011; Abdu et al., 2012) are used to study the evolution of plasma bubbles. Although many studies about the backscatter echoes beyond the foF2 have been studied, few studies are conducted to study the structure and evolution of plasma bubbles by ionosondes. In some cases, ionospheric irregularities could be observed by VHF radar when the range spread F occurred, but there are no backscatter echoes beyond the foF2 (strong spread F). Rodrigues et al. (2004) and Li et al. (2013) reported that backscatter plumes could be observed by VHF radar when range spread F occurred, but there are no backscatter echoes beyond the foF2 on ionograms. Thus, there might be a difference between the ionosonde backscatter plumes beyond the foF2 and the plumes observed by VHF radar. We think it might be worth studying the plasma bubbles by ionosonde backscatter plumes.

We reported the first observation of upwelling backscatter plumes with ionosondes at low latitudes on 13 March 2015. We know that the radar system with a single fixed beam is difficult to study the spatial structure of upwelling plumes. However, with the help of a pair of ionosondes and satellites flying side-by-side, it is also possible to study characteristics of the upwelling backscatter plumes associated with spread F/plasma bubbles by the beyond foF2 backscatter echoes with ionosondes.

2 Data sets

A pair of ionosondes was installed at Puer (PUR, 22.7° N, 101.05° E, Dip Lat 12.9° N) and Chiang Mai (CMU, 18.76° N, 98.93° E, Dip Lat 9.04° N) with a longitudinal separation of about 2.1° (about 225 km) were used to study the upwelling backscatter plumes. The ionosonde installed at PUR is a Wuhan Ionospheric Sounding System (WISS) developed by Wuhan University (Jiang et al., 2017; Shi et al., 2017). At a cadence of 5 min, the ionosonde system can carry out a range of vertical incidence ionospheric sounding from 2 MHz to 20 MHz. The ionosonde installed at CMU is the frequency-modulated continuous-wave (FMCW) ionosonde which is operated by the National Institute of Information and Communications Technology (NICT), Japan (Maruyama et al., 2007). With the help of the lower pair of Swarm A and C flying side-by-side at a mean altitude of about 450 km with longitudinal separation of about 1.4° (about 150 km) and observations of the all-sky imager installed at Qujing (25° N, 104° E, Dip Lat 15.1° N), the spatial structure of spread F/plasma bubbles can be identified in this study. The all-sky imager (Wu et al., 2018), with an integration time of 3 min, consists of a filter (630 nm) on a wheel, a fish-eye lens with a field of view of 180°, and a charge coupled device (CCD) detector with 1024 × 1024 pixels. The field of view of the imager is at an altitude of ~250 km.

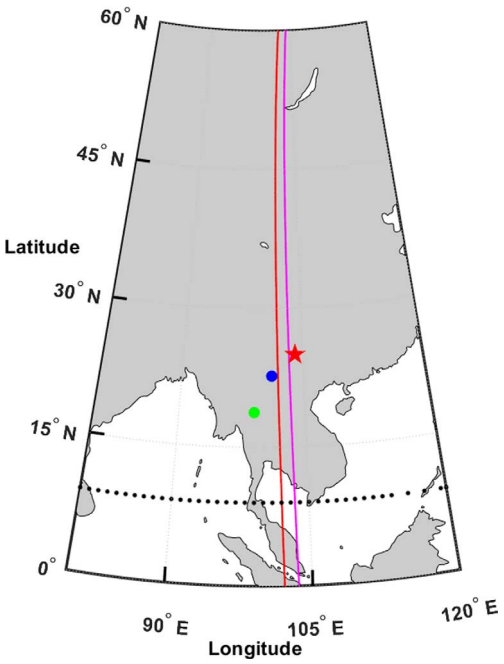

Fig. 1. Geophysical distribution of the pair of ionosondes (blue and green dots represent PUR and CMU, respectively), all-sky imager (red star), and the trace of the pair of Swarm A (the red solid line) and C (the magenta solid line) from ~13:03 UT to ~13:19 UT on 13 March 2015. The dotted backline represents the dip equator.

Figure 1 shows the geophysical distribution of the pair of ionosondes (blue and green dots represent PUR and CMU, respectively), the all-sky imager (red star), and the trace of the pair of Swarm A (the red solid line) and C (the magenta solid line). The dotted backline in Figure 1 represents the dip equator (with magnetic inclination $I = 0$ from International Geomagnetic Reference Field (IGRF) model).

3 Observations

Figure 2 shows observations of backscatter echoes on ionograms (red ellipses represent the echoes beyond the foF2) recorded at the PUR station on 13 March 2015. Although the

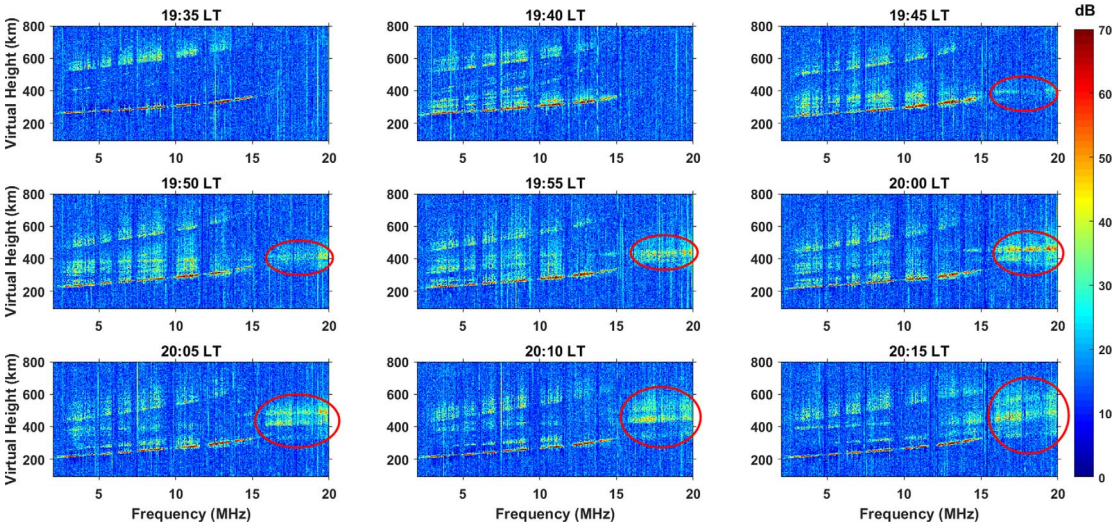

Fig. 2. Evolutions of ionograms (red ellipses represent the backscatter echoes beyond the foF2) recorded at PUR station on 13 March 2015.

main traces disappeared after about 15 MHz, an experienced operator could get the foF2 closer to the correct value by extrapolating the trace of the F2 layer (Jiang et al., 2020). In this study, we used the software tool ionoScaler (Jiang et al., 2017) to extrapolate the traces of the F2 layer to estimate the foF2 from ionograms. It can be seen from Figure 2 that "satellite" traces occurred at 19:40 LT (LT = UT + 7, applied for both PUR and CMU stations). It is noted that "satellite" traces, which appear as replicas of the usual F traces, are mainly produced by oblique reflections from the bottom side of the F layer (Tsunoda, 2005, 2008). Then, backscatter echoes beyond the foF2 can be observed at 19:45 LT. As the progress of the time, the strength (it represents the signal-noise ratio in this study) of backscatter echoes increases on the ionograms (from 19:45 LT to 20:00 LT, the maximum strength (the color represents the value of the signal-noise ratio) occurs at 20:00 LT) and then decreases (after 20:00 LT). In addition, we found that most of the backscatter echoes with frequencies larger than foF2 are almost horizontal (see Fig. 2). The horizontal characteristic suggests that backscatter echoes with different frequencies might be reflected from the same source (different scales irregularities in the same plumes). At the same time, although the traces of the F2 layer after about 15 MHz disappeared, it still can be seen that the main traces (below about 15 MHz) of the F2 region on ionograms do not diffuse or spread in Figure 2. Figure 3 shows evolutions of the associated ionograms recorded at CMU station on 13 March 2015. Due to the differences between these two ionosondes in the antenna and transmitter power, it can be seen that there are different strengths of the echoes in Figures 2 and 3. However, the backscatter echoes can still be seen on these ionograms. It can be seen from Figure 3 that the "satellite" traces started about 19:45 LT at CMU station. Similarly, the backscatter echoes (red ellipses) on the ionogram can be observed at about 19:55 LT. These backscatter echoes are beyond the foF2 as well in Figure 3. Similar to observation at PUR station but appears more evident, the main traces of the F2 region on ionograms do not diffuse or spread at CMU station (only "satellite" traces and backscatter plumes can be observed). Figure 4 shows latitudinal variations of electron density recorded by Swarms A (top pane) and C (bottom pane) from ~13:03 UT to ~13:19 UT on 13 March 2015. The blue and green lines represent the latitudes of PUR and CMU stations, respectively.

Figure 5 shows observations of airglow images from the all-sky imager at Qujing from 19:32:16 LT (LT = UT + 7) to 20:21:03 LT on 13 March 2015. The red star indicates the location of the imager. The blue and green dots represent the PUR and CMU stations. It can be seen from Figure 5 that a large plasma depletion (darkness) moved from CMU to PUR station. After about 19:50:21 LT, the large plasma depletion started to develop into many branches and stretched. At the same time, the plasma depletion moved eastward. Figure 6 is similar to Figure 5 but during 20:27:09 LT and 21:15:55 LT. Figure 6 shows that the plasma depletion continued to move eastward. At about 20:33:14 LT, a second plasma depletion occurred in the field of view of the all-sky imager and further moved eastward.

Figure 7 shows the range–time–intensify from ionograms at the PUR station at the frequency of 8, 13, 17, and 20 MHz on 13 March 2015. The echoes recorded at 8 and 13 MHz are below the foF2 (about 17 MHz from Fig. 2). The echoes recorded at 17 MHz are nearby the foF2. The echoes recorded at 20 MHz are beyond the foF2. The red line indicates the variation of the virtual base height of the ionosphere (h'F2). It can be seen from 8 and 13 MHz in Figure 7 that "satellite" traces can be observed frequently. Interestingly, the backscatter echoes from 17 and 20 MHz are similar to observations from VHF radar. There are also oscillations in the range–time–intensity. The upwelling backscatter plumes (marked by plume cluster A) can be observed and started about 19:45 LT. Similar to observations from Tsunoda (1983), backscatter strength increases during the growing phase of upward development. It also can be observed apparently from Figure 2 (from 19:40 LT to 20:00 LT). Moreover, resembling observations by VHF radar, backscatter plumes observed at 17 and 20 MHz occurred during the phase of downward movement of the ionosphere, compared with observations from 8 and 13 MHz. It also can be observed from the variations of h'F2. The upwelling backscatter plumes almost last for about 45 min (disappeared at 20:30 LT). After about 20:30 LT, the second backscatter plumes start to occur (marked by plume cluster B). It can be

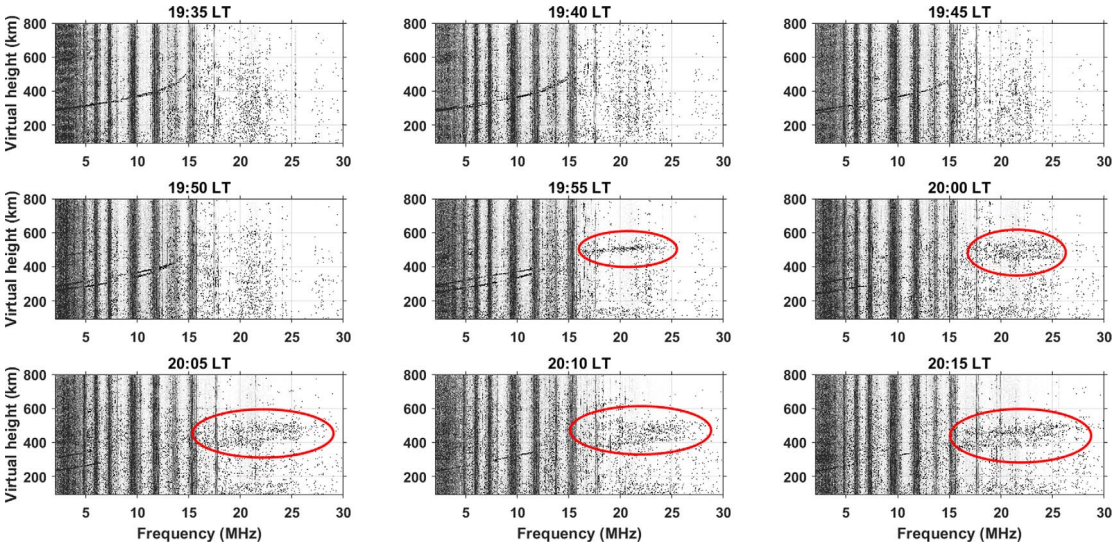

Fig. 3. Evolutions of ionograms (red ellipses represent the backscatter echoes beyond the foF2) recorded at CMU station on 13 March 2015.

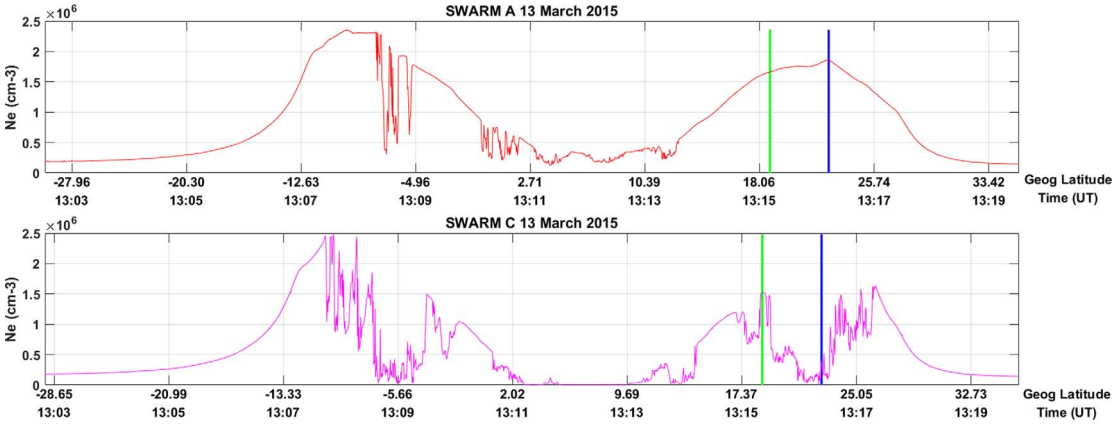

Fig. 4. Variations of electron density with latitude along the longitude of about 101 (top pane) and 104 (bottom pane) degree on 13 March 2015. The blue and green lines indicate, respectively, the position of PUR and CMU stations.

seen from Figure 6 that the second backscatter plumes mainly come from the west of PUR station.

4 Discussion

If we keep in mind that the beam of the electromagnetic wave transmitted by the antenna in the ionosonde system is wide, thus only a single station without the direction-finding system (ionosondes at PUR and CMU stations) is almost unable to identify the direction of the backscatter echoes observed with ionosondes in this study. Fortunately, with simultaneous observations of ionosondes, all-sky imager, and Swarm A and C, it is possible to estimate that the source of the backscatter echoes recorded at PUR and CMU stations. We know that these coherent backscatters should come from the direction perpendicular to the geomagnetic field lines. At off-equatorial latitude, the backscatter echoes should be mainly from the north direction in the north hemisphere.

Figure 5 shows that plasma depletions occurred north of the PUR station after about 19:44:21 LT. Interestingly, backscatter echoes started about 19:45 LT at PUR station. Observations verify that backscatter echoes might come from the north of PUR station at about 19:45 LT. Observations from VHF radar (Tsunoda, 1981, 1983) show that backscatter strength increases in the growing phase of upward development. Figure 2 shows that backscatter echoes strength increases from 19:45 LT to 20:00 LT. Figure 5 also shows the growing phase of plasma depletions from 19:38:21 LT to 20:02:45 LT. As a result, it is reasonable to think that the growing phase of upwelling backscatter plumes (see Fig. 7) is between 19:45 LT and 20:00 LT. Figure 5 indicates that the backscatter plumes started to move eastward after about 20:02:45 LT. At about 20:33:14 LT, the backscatter plumes is beyond the field of view of the ionosonde at PUR station (see Fig. 6). Therefore, during ~20:00 LT and ~20:30 LT (marked by plume cluster A), the backscatter plumes in Figure 7 are mainly from the northeast direction of the PUR station. Figure 1 shows that Swarm A nearly flew overhead PUR station at about ~13:15 UT. Swarm C was at the east (about 150 km) of PUR station at the same time. Interestingly, we found that plasma bubbles/irregularities were just recorded by Swarm C but not Swarm A in the

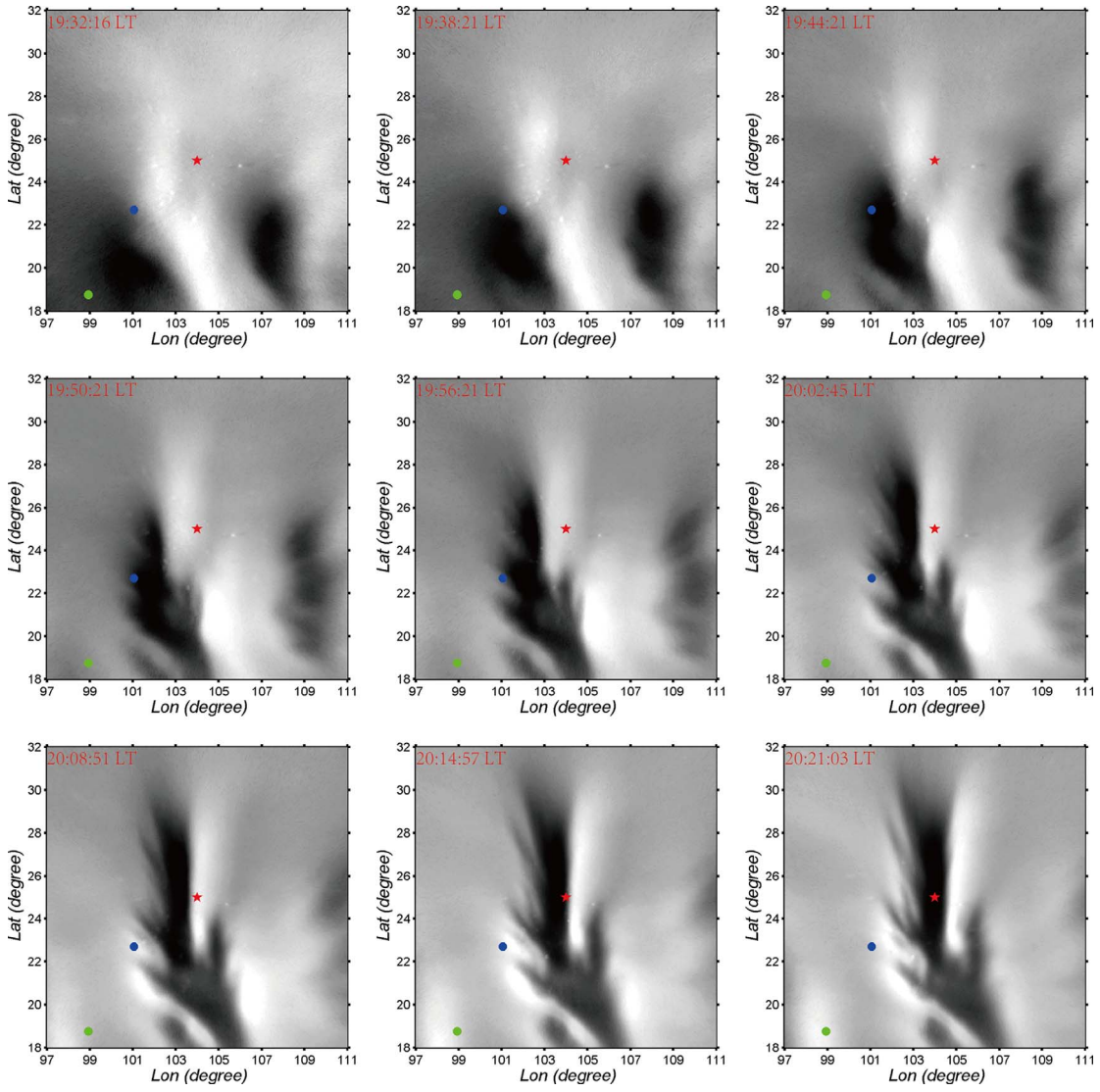

Fig. 5. Observations of airglow images from all-sky imager at Qujing station on 13 March 2015. The red star, blue, and green dots represent the all-sky imager, PUR, and CMU stations.

northern low-latitude region (nearby PUR and CMU stations), although Swarm A and C fly with a short separation of the longitude (about 1.4° corresponding to 150 km). Figure 5 shows that the movement of the irregularities is eastward. It can be seen that the irregularities moved away over Puer station (blue dot) and approached Qujing station (red star) about 20:14:57 LT. As a result, when Swarm A and C flew over the Puer and Qujing stations at about 20:16 LT, respectively, we can see that only Swarm C could observe the structure of the irregularities (see Fig. 4). Xiong et al. (2018) also reported a similar longitudinal thin structure of equatorial plasma depletions. Irregularities observed by Swarm C (see Fig. 4) further indicate that backscatter plumes are from the northeast of the PUR station. Tsunoda (2015, 2018) suggests that small-scale irregularities (less than 1 km) might be excited along the west wall of the upwelling. According to the backscatter mechanism, backscatter plumes at 17 and 20 MHz are associated with small-scale irregularities (~7.5 m to ~8.8 m, the half-wavelength ($\lambda/2$) of the working frequency), less than 1-km scale irregularities. Interestingly, we found that backscatter plumes observed at PUR station are from the west wall of the upwelling (see Fig. 5, from 19:44:21 LT to 20:02:45 LT). Moreover, secondary plumes (Tsunoda, 2015) excited along the west wall of the upwelling can be observed evidently by the ionosonde at PUR station (marked by plume cluster A in Fig. 7).

Furthermore, according to the direction of ionosonde backscatter plumes and magnetic inclination at the PUR station, we can estimate the altitudes of these backscatter echoes during the upwelling. Magnetic inclination at PUR station is about 32°, and the zenith is about 32°. We assume that ionosonde backscatter plumes are from the pure north direction during the growing phase (19:45 LT to 20:00 LT). Take plume cluster A, for example; the lowest and highest ranges of plume cluster A are ~400 km and ~460 km during 19:45 LT and 20:00 LT, respectively. The corresponding initial and peak altitudes are ~340 km and ~390 km. Then, the rising velocity is ~56 m/s. It is noted that the estimated altitudes and velocity of ionosonde backscatter plumes are rough due to the non-accurate direction

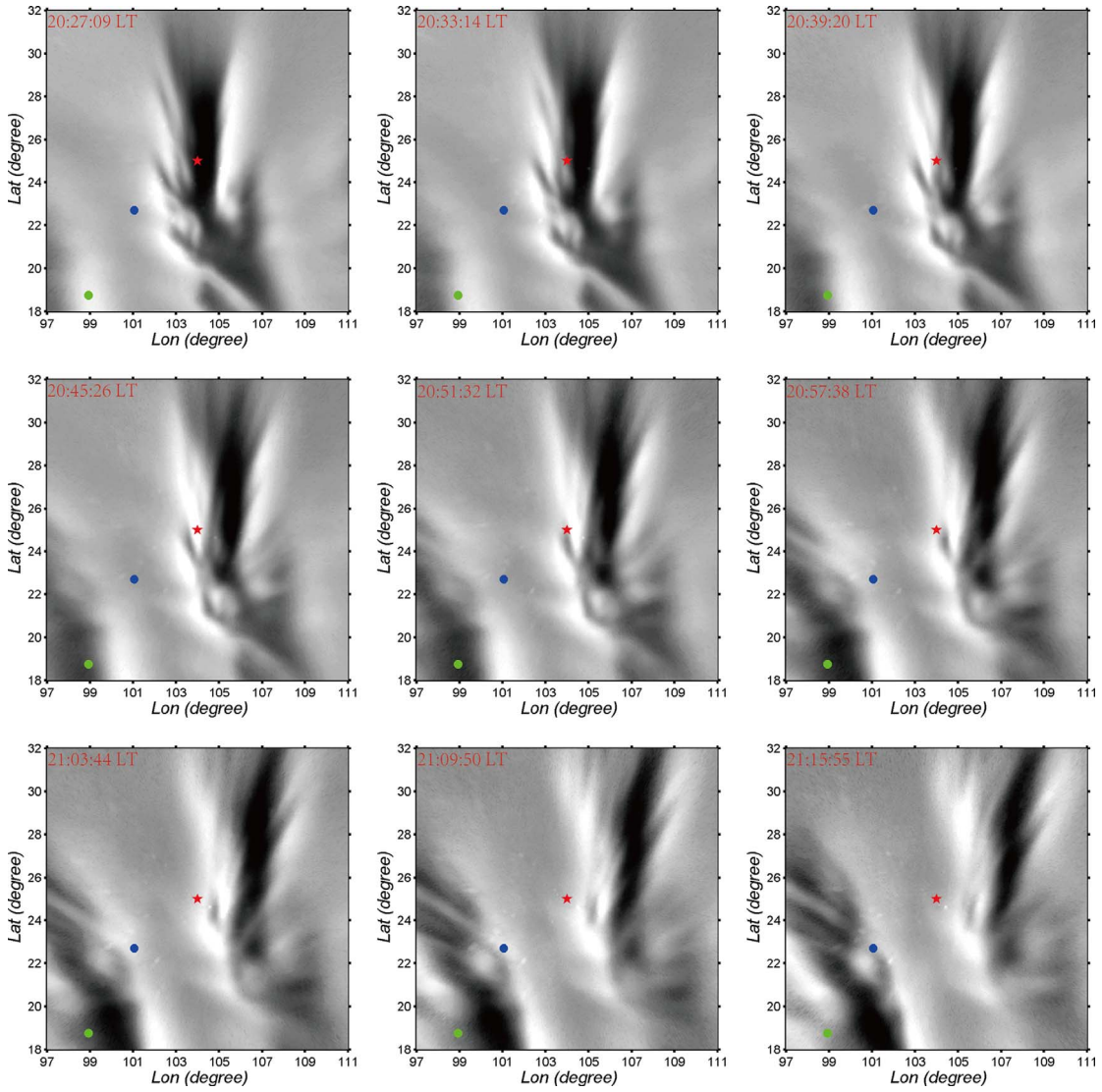

Fig. 6. Similar to Figure 5 but recorded during different local times.

of the backscatter plumes. However, the estimated altitudes and velocity are comparable to observations from VHF radar (Yokoyama & Fukao, 2006). Moreover, the estimated distances of backscatter echoes away from the PUR station is from ~210 km to ~243 km during the growing phase. The ground distance is ~400 km between PUR station (ionosonde) and Qujing station (all-sky imager). It can be seen from Figure 5 that the estimated distances of ionosonde backscatter plumes are reasonable from 19:45 LT to 20:00 LT.

Similar to PUR station, backscatter echoes observed at CMU station are mainly from the northeast direction. Due to it being far away from the upwelling, observations from the CMU station cannot capture the growing phase of the backscatter plumes. At about 19:55 LT, the backscatter plumes could be observed at CMU station. At this time, the plumes had almost reached their peak height and started to move eastward. That is the reason why the backscatter plumes did not resemble observations of the PUR station where the plumes moved upward. On the contrary, the plumes moved downward at CMU station at about 19:55 LT. The reason may be that the branches of plasma bubbles stretched close to the CMU station (see Fig. 5).

Tsunoda et al. (2018) suggested that the controlling driver for plasma bubbles development might be the local-scale upwelling growth but not the global-scale post-sunset rise (PSSR). When the upwelling/large-scale wave structure in the ionosphere occurs, the "satellite" traces on the ionogram can occur from oblique directions (Thampi et al., 2012). Compared with the strength of the "satellite" traces recorded at PUR and CMU stations, we can conclude that the large-scale wave structure might be closer to the PUR station than the CMU station. Figure 5 further verifies the hypothesis that the upwelling structure (darkness) was closer to the PUR station (from 19:32:16 LT to 19:38:21 LT). From 19:32:16 LT to 19:38:21 LT, it can be seen from Figure 5 that the upwelling (darkness) is between CMU and PUR stations (the distance is about 500 km). However, there are no "satellite" traces on ionograms recorded at CMU and PUR (about 19:35:00 LT in Figs. 2 and 3). It suggested that the upwelling/large-scale wave structure is a local-scale structure (less than about 500 km). Generally speaking,

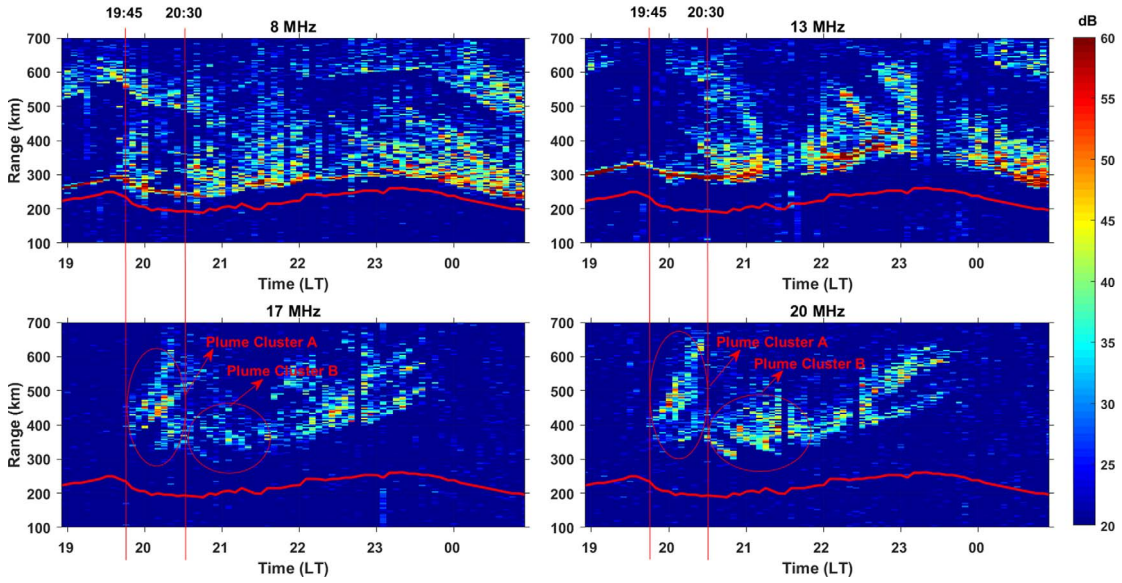

Fig. 7. Range–time–intensify from ionograms at PUR station at the frequency of 8, 13, 17, 20 MHz on 13 March 2015. The upwelling backscatter plumes marked by cluster A, and the descending backscatter plumes marked by cluster B. The red line indicates variations of h'F2.

the plasma bubble is initiated at the bottom side of the F layer above the magnetic equator and extends to higher altitudes and latitudes. However, the PUR station is located at magnetically middle latitude. We, therefore, assume that this local upwelling/large-scale wave structure might be from the lower atmosphere (gravity waves, etc.).

In terms of the descending backscatter plumes (marked by plume cluster B) in Figure 7, observations from the all-sky imager show that the ionosonde backscatter plumes originated from other regions and approached and receded to the PUR station (see Fig. 6). "Satellite" traces observed at 13 MHz around 20:30 LT further indicate that the echoes are approaching the ionosonde. Lynn et al. (2011) also reported these off-angle echoes to have approaching and receding characteristics by range–time displays. The second plume cluster (cluster B) in Figure 7 occurred at 20:30 LT and ended at about 22:00 LT. Figure 6 shows that the second plasma depletion with many branches comes close to Puer station at about 20:45 LT. Although the observations from the imager and ionosondes from 20:30 LT to 20:45 LT are different, the observations between 20:45 LT and 22:00 LT are almost consistent with the ionosonde and imager. During 20:30 LT and 20:45 LT, the Puer station is in the middle of the first and second plasma depletions (see Fig. 6), it is hard to specify if the backscatter echoes are from the first or second plasma depletions. That might be the reason why the observations from ionosonde and imager (20:30 LT to 20:45 LT) are different.

Observations of backscatter plumes beyond the foF2 at PUR station seem fairly well summarized by the cartoon given in Figure 8. It is noted that these coherent backscatters come from the direction perpendicular to the geomagnetic field lines (*B*-perpendicular direction). The yellow pane in Figure 8 indicates the north direction (*B*-perpendicular direction) of radio waves at the PUR station (off-equatorial latitude stations). The red curves represent ionospheric irregularities marked by plume cluster A and plume cluster B. The dot-black lines in the yellow pane represent the northwest, north, and northeast directions of radio waves transmitted from the PUR station. Figure 8 shows the movement of plume cluster A and cluster B, which is consistent with observations from the ionosondes and all-sky imager.

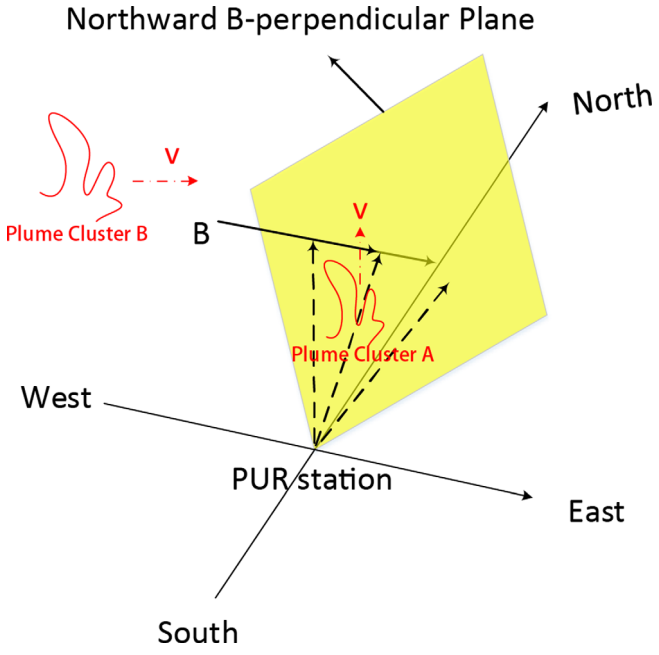

Fig. 8. Cartoon depictions for the evolutions of the ionosonde backscatter plumes. The yellow pane indicates the north direction (*B*-perpendicular direction) of radio waves at PUR station. The red curves represent ionospheric irregularities marked by plume cluster A and plume cluster B. The dot-black lines in the yellow pane represent the northwest, north, and northeast directions of radio waves transmitted from PUR station.

Simultaneous observations show that ionosonde backscatter plumes might have approaching and receding characteristics when it comes from other regions. However, when ionosonde backscatter plumes only have receding movement and their backscatter echoes increase, it suggests that the plumes might originate from the local region.

5 Conclusion

In this study, a pair of ionosondes (a longitudinal separation of about 2.1°, about 225 km), an all-sky imager, and the lower pair of Swarm A and C (a longitudinal separation of about 1.4°, about 150 km) were used to study the spatial characteristics of plasma bubbles/depletions. It is the first observation of upwelling backscatter plumes with ionosondes. Observations show that ionosonde backscatter plumes originated from a local-scale upwelling and moved eastward. Results show that ionosonde backscatter plumes are consistent with observations from VHF radars. The present study suggests that small-scale irregularities (about 10-m scale) can be observed by ionosondes and further used to study the evolution of plasma bubbles. It is necessary to complement the ionosonde data with simultaneous all-sky images and SWARM data to study the dynamics of the irregularities in this study. In addition, all-sky data are available only during nights without clouds and out of full moon periods. These conditions might restrict the possibility of a complete study of the irregularities using the present method. However, this study shows that some characteristics of the irregularities can be obtained from ionosonde backscatter plumes. Receding characteristics of ionosonde backscatter plumes suggest that they might originate from the local region when the strength of backscatter echoes increases, but plumes with both approaching and receding characteristics originate from other regions. It indicates that ionosonde backscatter plumes might give another opportunity to study the source of the upwelling associated with the spread of the F/plasma bubble in the ionosphere.

Acknowledgements. This work was supported by the National Natural Science Foundation of China (NSFC Nos. 42074184, 42104151, 41727804, and 41831073). The work of Jiyao Xu, Kun Wu, and Wei Yuan were supported by the Open Research Project of Large Research Infrastructures of CAS – "Study on the interaction between low/mid-latitude atmosphere and ionosphere based on the Chinese Meridian Project". Dip latitudes and Magnetic latitudes were calculated by IGRF-12 in this study. The Swarm data are provided by the European Space Agency (https://earth.esa.int/). Ionosonde data at CMU are from the National Institute of Information and Communications Technology (NICT) in Japan (http://seg-www.nict.go.jp/). We acknowledge the Institute of Earthquake Forecasting for providing ionosonde data at the PUR station. The ionosonde data at PUR and all-sky imager data at Qujing used in this study are available from Zenodo: https://zenodo.org/record/4663614 (DOI: 10.5281/zenodo.4663614, the section: Ionosonde Backscatter Plumes). The editor thanks two anonymous reviewers for their assistance in evaluating this paper.

References

Abdu MA, Batista IS, Reinisch BW, MacDougall JW, Kherani EA, Sobral JHA. 2012. Equatorial range spread F echoes from coherent backscatter, and irregularity growth processes, from conjugate point digital ionograms. *Radio Sci* **47**: RS6003. https://doi.org/10.1029/2012RS005002.

Argo PE, Kelley MC. 1986. Digital ionosonde observations during equatorial spread F. *J Geophys Res* **91(A5)**: 5539–5555. https://doi.org/10.1029/JA091iA05p05539.

Fukao S, Hashiguchi H, Yamamoto M, Tsuda T, Nakamura T, Yamamoto MK, Sato T, Hagio M, Yabugaki Y. 2003. Equatorial atmospheric radar (EAR): System description and first results. *Radio Sci.* **38(3)**: 1053. https://doi.org/10.1029/2002RS002767.

Jiang C, Wei L, Lan T, Yang G, Liu J, Zhao Z. 2020. A statistical study of autoscaled data at the northern equatorial ionization anomaly during the year 2016. *Radio Sci* **55**: e2019RS006898. https://doi.org/10.1029/2019RS006898.

Jiang C, Yang G, Zhou Y, Zhu P, Lan T, Zhao Z, Zhang Y. 2017. Software for scaling and analysis of vertical incidence ionograms-ionoScaler. *Adv Space Res* **59**: 968–979. https://doi.org/10.1016/j.asr.2016.11.019.

Kelley MC, Larsen MF, La Hoz C, McClure JP. 1981. Gravity wave initiation of equatorial spread F: A case study. *J Geophys Res* **86**: 9087.

Li G, Ning B, Abdu MA, Otsuka Y, Yokoyama T, Yamamoto M, Liu L. 2013. Longitudinal characteristics of spread F backscatter plumes observed with the EAR and Sanya VHF radar in Southeast Asia. *J Geophys Res Space Phys* **118**: 6544–6557. https://doi.org/10.1002/jgra.50581.

Li G, Otsuka Y, Ning B, Abdu MA, Yamamoto M, Wan W, Liu L, Abadi P. 2016. Enhanced ionospheric plasma bubble generation in more active ITCZ. *Geophys Res Lett* **43**: 2389–2395. https://doi.org/10.1002/2016GL068145.

Lynn KJW, Otsuka Y, Shiokawa K. 2011. Simultaneous observations at Darwin of equatorial bubbles by ionosonde-based range/time displays and airglow imaging. *Geophys Res Lett* **38**: L23101. https://doi.org/10.1029/2011GL049856.

Maruyama T, Kawamura M, Saito S, Nozaki K, Kato H, Hemmakorn N, Boonchuk T, Komolmis T, Ha Duyen C. 2007. Low latitude ionosphere-thermosphere dynamics studies with ionosonde chain in Southeast Asia. *Ann Geophys* **25(7)**: 1569–1577. https://doi.org/10.5194/angeo-25-1569-2007.

Otsuka Y, Shiokawa K, Ogawa T, Yokoyama T, Yamamoto M, Fukao S. 2004. Spatial relationship of equatorial plasma bubbles and field-aligned irregularities observed with an all-sky airglow imager and the Equatorial Atmosphere Radar. *Geophys Res Lett* **31**: L20802. https://doi.org/10.1029/2004GL020869.

Rodrigues FS, de Paula ER, Abdu MA, Jardim AC, Iyer KN, Kintner PM, Hysell DL. 2004. Equatorial spread F irregularity characteristics over São Luís, Brazil, using VHF radar and GPS scintillation techniques. *Radio Sci* **39**: RS1S31. https://doi.org/10.1029/2002RS002826.

Sales GS, Reinisch BW, Scali JL, Dozois C, Bullett TW, Weber EJ, Ning P. 1996. Spread *F* and the structure of equatorial ionization depletions in the southern anomaly region. *J Geophys Res* **101 (A12)**: 26819–26827. https://doi.org/10.1029/96JA01946.

Shi JK, Wang GJ, Reinisch BW, Shang SP, Wang X, Zherebotsov G, Potekhin A. 2011. Relationship between strong range spread F and ionospheric scintillations observed in Hainan from 2003 to 2007. *J Geophys Res* **116**: A08306. https://doi.org/10.1029/2011JA016806.

Shi S, Yang G, Jiang C, Zhang Y, Zhao Z. 2017. Wuhan ionospheric oblique backscattering sounding system and its applications – A review. *Sensors* **17(6)**: 1430, 1–23. https://doi.org/10.3390/s17061430.

Thampi SV, Tsunoda RT, Jose L, Pant TK. 2012. Ionogram signatures of large-scale wave structure and their relation to equatorial spread *F*. *J Geophys Res* **117**: A08314. https://doi.org/10.1029/2012JA017592.

Tsunoda RT. 1981. Time evolution and dynamics of equatorial backscatter plumes 1. Growth phase. *J Geophys Res* **86(A1)**: 139–149. https://doi.org/10.1029/JA086iA01p00139.

Tsunoda RT. 1983. On the generation and growth of equatorial backscatter plumes: 2. Structuring of the west walls of upwellings. *J Geophys Res* **88(A6)**: 4869–4874. https://doi.org/10.1029/JA088iA06p04869.

Tsunoda RT. 2005. On the enigma of day-to-day variability in equatorial spread F. *Geophys. Res. Lett.* **32**: L08103. https://doi.org/10.1029/2005GL022512.

Tsunoda RT. 2008. Satellite traces: An ionogram signature for large-scale wave structure and a precursor for equatorial spread F. *Geophys. Res. Lett.* **35**: L20110. https://doi.org/10.1029/2008GL035706.

Tsunoda RT. 2015. Upwelling: A unit of disturbance in equatorial spread F. *Prog Earth Planet Sci* **2**: 9. https://doi.org/10.1186/s40645-015-0038-5.

Tsunoda RT, Saito S, Nguyen TT. 2018. Post-sunset rise of equatorial *F* layer – or upwelling growth? *Prog Earth Planet Sci* **5**: 22. https://doi.org/10.1186/s40645-018-0179-4.

Woodman RF, La Hoz C. 1976. Radar observations of *F* region equatorial irregularities. *J Geophys Res* **81(31)**: 5447–5466. https://doi.org/10.1029/JA081i031p05447.

Wright JW, Argo PE, Pitteway MLV. 1996. On the radiophysics and geophysics of ionogram spread *F*. *Radio Sci* **31(2)**: 349–366. https://doi.org/10.1029/95RS03104.

Wu K, Xu J, Xiong C, Yuan W. 2018. Edge plasma enhancements of equatorial plasma depletions observed by all-sky imager and the C/NOFS satellite. *J Geophys Res Space Phys* **123**: 8835–8849. https://doi.org/10.1029/2018JA025809.

Xiong C, Xu J, Wu K, Yuan W. 2018. Longitudinal thin structure of equatorial plasma depletions coincidently observed by Swarm constellation and all-sky imager. *J Geophys Res Space Phys* **123**: 1593–1602. https://doi.org/10.1002/2017JA025091.

Yokoyama T, Fukao S. 2006. Upwelling backscatter plumes in growth phase of equatorial spread *F* observed with the equatorial atmosphere radar. *Geophys Res Lett* **33**: L08104. https://doi.org/10.1029/2006GL025680.

Cite this article as: Jiang C, Wei L, Yokoyama T, Xu J, Wu K, et al. 2022. Upwelling coherent backscatter plumes observed with ionosondes in low-latitude region. *J. Space Weather Space Clim.* **12**, 13. https://doi.org/10.1051/swsc/2022010.